Mid-infrared rotated image singly resonant twisted rectangle optical parametric oscillator based on HgGa$_2$S$_4$ pumped at 1064 nm

Georgi Marchev,[1] Manuel Reza,[1,2] Valeriy Badikov,[3] Adolfo Esteban-Martin,[1,4] Georg Stöppler,[5] Marina Starikova,[1,6] Dmitrii Badikov,[3] Vladimir Panyutin,[1,3] Marc Eichhorn,[5] Galina Shevyrdyaeva,[3] Aleksey Tyazhev,[1] Svetlana Sheina,[3] Antonio Agnesi,[2] Anna Fintisova,[3] and Valentin Petrov[1,*]

[1]Max-Born-Institute for Nonlinear Optics and Ultrafast Spectroscopy, 2A Max-Born-Str., 12489 Berlin, Germany

[2]Università di Pavia, Dip. Ingegneria Industriale e dell'Informazione, via Ferrata 3, 27100 Pavia, Italy

[3]High Technologies Laboratory, Kuban State University, 149 Stavropolskaya Str., 350040 Krasnodar, Russia

[4]ICFO-Institut de Ciencies Fotoniques, Mediterranean Technology Park, 08860 Castelldefels, Barcelona, Spain

[5]French–German Research Institute of Saint-Louis (ISL), 5 rue du Général Cassagnou, BP 70034, 68301 Saint Louis Cedex, France

[6]Special Technologies, Ltd., 1/3 Zeljonaja gorka Str., 630060 Novosibirsk, Russia

*Corresponding author: petrov@mbi-berlin.de

We compare linear, planar ring, and rotated image singly resonant twisted rectangle (RISTRA) type nanosecond optical parametric oscillator cavities using HgGa$_2$S$_4$ nonlinear crystal pumped by 8 ns pulses at 1064 nm from a low beam quality pump source. The input–output characteristics and the output idler beam quality at 6300 nm are compared for two values of the pump beam diameter presenting different cavity Fresnel numbers and magnitudes of the spatial walk-off effect due to birefringence. The RISTRA cavity ensures in all cases a circular output beam profile but is advantageous in terms of beam quality with respect to the planar ring only at a large pump beam diameter.   © 2014 Optical Society of America

OCIS codes: (190.4970) Parametric oscillators and amplifiers; (190.4360) Nonlinear optics, devices; (190.4400) Nonlinear optics, materials.

http://dx.doi.org/10.1364/AO.53.007951

1. Introduction

Nanosecond optical parametric oscillators (OPOs) are widely used to convert the wavelength of powerful laser sources emitting in the near-IR part of the spectrum to longer wavelengths in the mid-IR [1]. Nondegenerate operation is necessary to obtain long enough idler wavelengths, and this is realized in singly resonant OPOs. As usual, the pump (P), signal (S), and idler (I) wavelengths follow the convention $\lambda_I \geq \lambda_S > \lambda_P$. Whether the signal or idler is of main interest, there are good reasons for which the signal is normally chosen to be the resonated wave in such mid-IR OPOs [1]. The idler is then produced in single or double pass through the nonlinear crystal and then fully extracted.

One of the greatest challenges in scaling nanosecond OPOs to high energy is the output beam quality. On the one hand, because of damage threshold

constraints, OPO energy scaling implies increasing the beam diameters while keeping the pump fluence unchanged. On the other hand, the cavity length should be as short as possible to enable more round-trips. In a singly resonant OPO with a high Fresnel-number (defined here by $N_F = 4w_S^2/\lambda_S L$, where L denotes the cavity length and w_S is the resonated signal waist) cavity that supports many transverse modes, the output beam quality is often poor. Because in cavities with flat mirrors different portions of the beams uncouple and develop more or less independently of one another, uncorrelated phase and amplitude variations occur across the beam profile, resulting in poor beam quality [2]. One of the methods developed to establish correlation among all regions of the beams, resulting in more uniform phase and amplitude, exploited the spatial walk-off between signal and idler in birefringent nonlinear crystals, combined with image rotation [2]. This idea stimulated the development of three-dimensional cavity designs.

Spatial walk-off tends to smooth the phase of the resonated signal beam over regions that interact with a particular portion of the idler beam, and uniform phase can be achieved parallel to the walk-off direction [2]. By rotating the image by 90° on each cavity pass, one can induce a uniform phase across the entire beam with correlation in both transverse directions. Image rotation can be accomplished in different ways: one compact design is a three-dimensional four-mirror ring, named a rotated image singly resonant twisted rectangle (RISTRA) [3]. Such nonplanar geometry is insensitive to small tilts of the cavity mirrors; thus RISTRA requires no cavity mirror adjustments and can be engineered as a monolithic block. Each image rotation also rotates the polarization of the resonated signal; hence, a half-wave plate compensates for this effect in each round-trip.

Initially, RISTRA was proposed for type-II phase matching (nonparallel Poynting vectors of signal and idler) in the nonlinear crystal. Image rotation modeling (developed only for single-frequency operation) was presented for type-II eoo (symbols follow λ_I, λ_S, λ_P) phase matching in KTiOPO$_4$ (KTP) in a singly resonant OPO pumped at $\lambda_P = 1064$ nm [2]. In this case, the idler walk-off angle ρ_I amounts to 36 mrad, which gives, for the 30 mm crystal length and 3.4 mm pump diameter, a spatial walk-off of 32%. From simple simulation for two times above threshold OPO operation when only the signal wave is resonated, it was concluded that the effect of image rotation was responsible for the transfer of the good beam quality (low divergence and M^2 parameter), due to the large spatial walk-off, from the critical plane (as computed for a planar ring without image rotation) to the noncritical plane when image rotation is introduced. It is very interesting that equal improvement of the nonresonated idler quality (as for the signal), which in fact is produced in single pass intracavity difference-frequency generation, was predicted.

However, subsequent experimental verification focused on the signal properties only. In [4], the

15-mm-long KTP crystal was used again in type-II phase matching, but this time oeo (i.e., the resonated signal and not the idler was decoupled from the pump) with $\lambda_P = 532$ nm. The signal walk-off amounted then to 48 mrad, giving a spatial walk-off of 33% relative to the 2.2 mm pump diameter. The understanding is that the RISTRA concept is most effective using pump beams in the fundamental mode with single-frequency OPO operation, which requires single-frequency operation of the pump laser as well. At four times above the OPO threshold the signal M^2 was improved to 1.6–1.7 for Fresnel numbers of 33–45 [3] with image rotation, which is slightly worse than the critical plane value but much better than the noncritical plane value in an equivalent planar ring without image rotation. Using pump beams that were not in fundamental mode (M$^2 \sim 1.9$) and larger pump diameters (5 mm) was also studied in [3] with the same OPO at Fresnel numbers as large as 300. Exactly in such high Fresnel-number OPOs, where the pump beam is sometimes transformed into a nearly top-hat spatial profile to overcome damage limitations for the nonlinear crystal, RISTRA seems to be a very important concept. With such a low-quality pump beam, the optimum polarization configuration for KTP was considered to be oeo, which ensures decoupling of the signal not only from the idler but also from the pump, while the idler can carry away phase distortions of the pump [3]. These arguments concern the beam quality of the resonated signal, however, for which M$^2 \sim 3$ was achieved at four times above threshold OPO operation. The performance degraded when the OPO was not single frequency (no seeding applied at the signal wavelength) and got worse when the pump laser was unseeded: the beam quality of the signal wave was deteriorated by backconversion associated with the spikes in pump power caused by beating of longitudinal modes. Nevertheless, most of the subsequent experiments were not performed in the single-frequency regime.

If, in a type-II OPO, the idler is the wave with polarization opposite to that of the pump; then pump distortions are partially imprinted on the signal. Finally, the worst scenario for the signal beam quality was numerically predicted for type-I phase matching when the signal and idler are parallel and both walk-off from the pump [3]. However, later on, the RISTRA design turned out to also be effective for type-I phase matching [5,6].

While the "ideal" conditions associated with the RISTRA concept mentioned above could be more or less fulfilled for the signal output in the case of KTP (or related) nonlinear crystals, moving to longer idler wavelengths in the mid-IR, it becomes impossible, difficult, or impractical to satisfy some of them. Restrictions arise from the nonoxide nonlinear crystal properties or the optical elements. Thus, in the ZnGeP$_2$ (ZGP) RISTRA OPO described in [5,6], only type-I eeo phase matching was possible for the targeted $\lambda_S = 3400$ nm; the signal was not decoupled

from the idler, and the spatial walk-off angle was ~4 times smaller compared to KTP. As a consequence, this RISTRA OPO pumped near 2 μm exhibited >11 times lower ratio of the spatial walk-off to pump diameter compared with the above-discussed KTP-based OPOs. In addition, while the fundamental pump beam transversal mode was available, neither the pump nor the OPO operated single frequency. Nevertheless, impressive results were obtained with ZGP [5,6], in particular very good signal beam quality at high conversion efficiency. However, no information on the idler and no comparison with an equivalent planar ring or linear cavity in order to understand the underlying effect were presented.

Although moving away from degeneracy to $\lambda_I \sim$ 6450 nm [7,8], type-II oeo phase matching in 2 μm pumped ZGP is also possible, type-I eeo was still chosen in that experiment. Additional difficulties arise, however, if the idler is of main interest (which is often the case in OPOs). Resonating the idler means lower intracavity power and larger waist [9], i.e., relaxed thermal problems as well as reduced damage probability for the nonlinear crystal since separation from the band-gap is larger. However, it is challenging to make the idler a resonating wave for a few reasons: (i) cavity mirrors in the mid-IR, keeping in mind the broader tuning range, are problematic for fabrication and have low damage resistivity with characteristics for signal and pump wavelengths which are difficult to optimize; and (ii) although better damage resistivity of the nonlinear crystal can be expected far from the band-gap, the residual absorption at the idler wavelength (as in the experiments described here) may lead to excessive heating.

The type-I eeo ZGP OPO pumped near 2 μm described in [7,8] was the only RISTRA configuration for which the properties of the nonresonated mid-IR idler wave were investigated. Excellent results with respect to M^2 were obtained both for signal and idler, but no systematic comparison with other cavities to highlight the reasons was undertaken. The only comparison mentioned was with a short (42 mm) linear cavity pumped in single pass, with double pass for the idler and a 50% OC for the signal while all other parameters were kept similar [7]. In this case an idler energy of 4 mJ at 6450 nm was generated for pump energy of 44 mJ (2.9 times above threshold) with lower $M^2 = 2.75$ in the noncritical plane compared to $M^2 = 6.6$ in the critical plane.

All these open questions related to the applicability of the RISTRA concept in the mid-IR spectral range, the role of the spatial walk-off and type of phase matching, and in particular the properties of the nonresonated idler wave served as motivation for this work. Our interest was focused, however, on 1 μm pumped OPOs based on wide band-gap non-oxide crystals that are capable of generating directly mid-IR idler wavelengths above the 4–5 μm limit of oxides [1].

2. Experimental Setup

$HgGa_2S_4$ (HGS) is one of the most promising candidates for mid-IR OPOs pumped at $\lambda_P = 1064$ nm. With this crystal we demonstrated the highest idler energy from such an OPO converting 1064 nm to the mid-IR above 5 μm, achieving 3 mJ at 6300 nm in ~7 ns-long idler pulses at a repetition rate of 10 Hz [10]. This linear singly resonant OPO was pumped in double pass, while the idler was also totally out-coupled after a double pass. Unfortunately, although the physical cavity length was intentionally increased to 52 mm to improve the beam quality, the measured M^2 for the idler was of the order of 30 [10]. Thus, our goal in this work was to improve the output beam quality, relying basically on the same pump source and similar samples, by investigating different cavity configurations.

Comparing HGS to the commercially available chalcopyrite $AgGaS_2$ (AGS), the standard nonoxide mid-IR material for 1 μm pumped OPOs [1], its nonlinear coefficient d_{36} is ~1.8 times higher, and this at a slightly increased band-gap value (2.79 eV for HGS against 2.7 eV for AGS), i.e., at somewhat higher damage resistivity [11]. Due to its wide band-gap, HGS, similar to AGS, can be pumped at 1064 nm without any two-photon absorption.

Note that defect chalcopyrites of this type possess a second nonzero tensor component d_{31}, but the unknown relative sign in HGS does not allow one to utilize it for increasing the effective nonlinearity d_{eff} by optimizing the azimuthal angle φ. In [5] it was argued that type-I phase matching would also be effective in the RISTRA cavity due to the four reflections of the signal only. However, there are no arguments that when both types of phase matching are possible, type-I shall be better, and as already mentioned, in this paper the authors addressed only the beam quality of the resonated signal. Since this is the situation with HGS pumped near 1 μm and d_{eff} is higher for type-II eoe phase matching, the azimuthal angle cut was chosen to be $\varphi = 0°$. It shall be outlined that the condition of decoupling the idler from both the pump and the signal is impossible to realize with the optically negative HGS because the oee polarization configuration is not phase matchable (from the nonoxide nonlinear crystals that can be pumped at 1064 nm, this is possible only in Ag_3AsS_3 at the price of greatly reduced d_{eff} [1]). Therefore, for HGS pumped at 1064 nm, there is no alternative to resonating the signal in a type-II eoe phase-matching scheme.

In the present study, the idea was also to employ a commercial pump source with relatively poor beam quality oscillating on many longitudinal modes, in fact the same one as in [10]. The pump source was a diode-pumped Q-switched Nd:YAG laser/amplifier (Innolas) emitting ~8 ns pulses with a bandwidth ~1 cm^{-1} and maximum energy of 250 mJ at 1064 nm, at a nominal repetition rate of 100 Hz. After an attenuator consisting of a wave plate and a polarizer, the polarization state of the pump beam was horizontal,

which defines the critical or the walk-off plane in the optically negative HGS, while vertical will be the noncritical plane. To improve the spatial beam profile (eliminate diffraction rings producing hot spots), a vacuum diamond pinhole was installed in the focus of a telescope. The pump M^2 parameter measured behind the telescope amounted to ~ 2. The beam size (at e^{-2} intensity level) was reduced by a second telescope to $D_P = 2.25$ mm (small diameter) for the first series of measurements, while it was $D_P = 5.35$ mm (large diameter, comparable to the HGS crystal aperture) without this telescope for the second series of measurements; see Fig. 1. The repetition rate was reduced to 10 Hz in both cases, either by a mechanical shutter synchronized to the internal Pockels cell driver of the laser or by driving the Pockels cell at 10 instead of 100 Hz although the pump diodes were operated at 100 Hz. The adopted repetition rate of 10 Hz ensures that thermal lensing effects on M^2 can be ignored [12]. The two series of measurements correspond to different ratios of the spatial walk-off to the pump beam diameter in order to highlight this effect.

We wanted to compare a linear (standing-wave) cavity with a RISTRA cavity, but studied in addition a planar ring cavity with spatial walk-off only in the horizontal (critical) plane as an intermediate case; the last two are schematically shown in Fig. 2. All cavities were singly resonant for the signal at $\lambda_S \sim$ 1280 nm and pumped in single pass. The mirror characteristics of the input couplers (ICs) and output

Fig. 2. RISTRA (top) and planar ring (bottom) OPO cavities investigated. IC, input coupler; OC, output coupler; BM, bending mirror; R, reflectivity.

couplers (OCs) at different wavelengths were optimized for an incidence angle of 32.8°, because they were designed for the RISTRA monolithic cavity, whose mirror holes are prealigned and fixed. The linear cavity consisted just of an IC and an OC, while the bending mirrors (BMs) used in the ring cavities (Fig. 2) were of the same kind as the ICs.

Two different sets of mirrors were used in the two series of measurements with small and large pump beam sizes; however, the same mirrors were used in comparing the three cavities. Nevertheless, the mirror characteristics were slightly different because the angle of incidence was 0° in the linear cavity, $\sim 30°$ in the three-mirror equilateral planar ring cavity, and 32.8° in the RISTRA cavity. Also the polarization of the different waves was different in the planar ring and RISTRA cavities; thus, OCs were used in p polarization (idler) and s polarization (signal) in the planar ring cavity, but the situation was opposite in the RISTRA cavity. The ICs when used as BMs operated for s polarization (signal) in the planar ring cavity and for both polarizations in the RISTRA cavity. Although we were interested solely in the nonresonated idler, the OCs were partially transmitting for the signal in order to avoid damage to the nonlinear crystal caused by the high intracavity energy trapped: in the different configurations R_S(OC) varied between 66% and 80%. The extraction of the idler through the OC was also different, between 83% and 95%. The ICs were highly reflecting the signal and highly transmitting the pump but with slight differences. Finally, the number of mirrors was different in the three cavities, and in comparison to the other two, the RISTRA configuration contained a half-wave plate ($\lambda/2$) for compensation of the signal polarization rotation. To be able to compare the results we normalized them to pump energy incident on the HGS crystal and tried to operate the different OPOs at the same level above threshold. From the numerous experiments performed we can conclude that the above-mentioned inevitable differences in
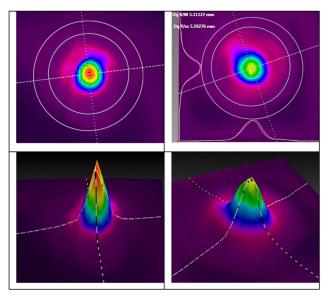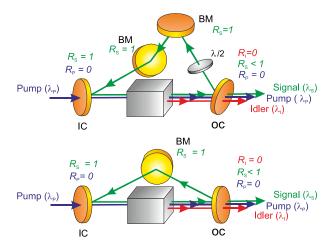
Fig. 1. 2D (top) and 3D (bottom) pump beam profiles in the OPO position with additional telescope (left) and with only the vacuum aperture telescope (right). In the first case Gaussian fits give $2w_{PV} \approx 2.4$ mm and $2w_{PH} \approx 2.1$ mm in the vertical (V) and horizontal (H) planes, respectively, or an average diameter of $D_P = 2.25$ mm. In the second case the corresponding values are $2w_{PV} \approx 5.1$ mm, $2w_{PH} \approx 5.6$ mm, and $D_P = 5.35$ mm. The exact values correspond to the eigenaxes determined by the software, shown by white lines, which are only approximately vertical and horizontal.

the characteristics of the optical elements can still be considered tolerable in pulsed nanosecond OPOs.

The physical length of the monolithic RISTRA cavity was $L = 128$ mm, but what was equal for all cavities, for comparison, was the round-trip optical length $L*$, i.e., the number of round-trips for the resonated signal wave. To this aim we took into account the double pass through the crystal in the linear cavity, although the second pass was unpumped.

Two similar orange-phase HGS crystals with parallelism of 15″ were used in the two series of experiments. Their input and output faces were antireflection (AR) coated with a single quarter-wave layer for the signal, which was also effective for the pump wave, while the reflection losses for the idler corresponded to the Fresnel reflection. One crystal (HGS #2) had a length of $l = 13.44$ mm and an aperture of 10 mm × 10 mm, and the other one (HGS #3) had $l = 17.88$ mm and an aperture of 8.57 mm × 7 mm. The origin of the bulk absorption in the mid-IR above ∼5 µm, which can be seen in Fig. 3, is still unclear because it is known that HGS can have clear transparency up to at least 8 µm [11].

3. Input–Output OPO characteristics

As already mentioned, we characterized primarily the idler output of the OPOs, while the signal and the residual pump were suppressed behind the OC by suitable mirrors and filters. All results in terms of output energy were corrected for the transmission of these elements at the idler wavelength. The external quantum conversion efficiency was calculated from the idler energy. Normally this would give lower values compared to estimations based on the signal output. The reason is that the idler was not perfectly extracted for few reasons: Fresnel reflections and bulk absorption in the HGS crystals as well as <100% transmission of the OC. Finally, for simplicity we confined the present comparison to normal incidence on the nonlinear crystal and collinear interaction, which produced an idler wavelength of $\lambda_I = 6300$ nm.

A. Short Linear Cavity

A short linear cavity of $L = 23$ mm physical length was used in a preliminary experiment to compare the two samples and their homogeneity. The small pump beam size, $D_P = 2.25$ mm, chosen in this experiment also permitted us to map the crystal aperture. The crystals were not homogeneous, and the output energy varied down to about 50% of the maximum value. The sample HGS #3 had better overall uniformity. The results below correspond approximately to the best positions in the two crystals.

Figure 4 shows the idler energy and the quantum conversion efficiency q obtained versus the pump pulse energy. The upper abscissa gives the average pump fluence calculated, which is equal to ½ of the peak axial value. The idler slope efficiency η is calculated from the linear fits shown. More reasonable thresholds than those depending on detector sensitivity are obtained in such OPOs from linear extrapolation of these linear fits. It can be seen from Fig. 4 that the slopes are equal for the two crystals and only the threshold is somewhat lower for HGS #2: roughly 2 mJ compared to 2.5 mJ for HGS #3. This was a little unexpected since this crystal was shorter but can be attributed to more inhomogeneities along the crystal length.

Some saturation of the quantum conversion efficiency is seen at high pump energies, starting from about three times threshold. This might be an indication of backconversion in the temporal and spatial maxima of the beams because the quantum conversion efficiency is calculated in terms of energy, i.e., with integral values. As already mentioned the idler extraction was not perfect and the actual pump depletion could substantially exceed the calculated quantum conversion efficiency [10]. Nevertheless, the maximum value in Fig. 4 is 2.2 times larger than the highest quantum conversion efficiency achieved with the double pump/idler pass, singly resonant linear OPO, which produced 3 mJ at 6300 nm in [10], with a similar HGS sample.

B. Different Cavities with Small Pump Beam Diameter

Figure 5 shows the obtained input–output OPO characteristics with the three cavities at small pump
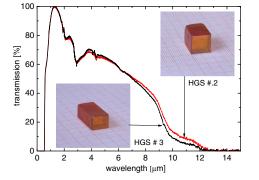

Fig. 3. Measured unpolarized transmission of the two HGS samples used.
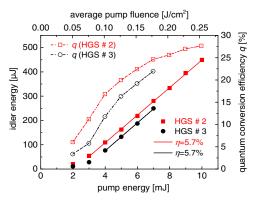

Fig. 4. Idler energy and quantum conversion efficiency obtained with HGS #2 and HGS #3 in a short linear OPO cavity.
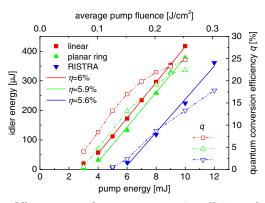
Fig. 5. Idler energy and quantum conversion efficiency obtained with HGS #2 and $D_P = 2.25$ mm in linear, planar ring, and RISTRA cavities.

Fig. 6. Idler energy and quantum conversion efficiency obtained with HGS #3 and $D_P = 5.35$ mm in linear, planar ring, and RISTRA cavities. An additional case of a planar ring cavity with a half-wave plate is also included.

diameter ($D_P = 2.25$ mm). In this case HGS #2 was used and the linear cavity length was 54.5 mm. For all three cavities damage to the cavity mirrors (both IC and OC on ZnSe substrate) was the limiting factor for the pump level.

For the linear cavity, the OPO threshold increased by roughly 50% compared to the short cavity studied in the previous subsection due to the decreased number of round-trips, while the slope efficiency became slightly higher. The extrapolated thresholds for the three cavities were 3, 3.5, and 5.6 mJ, respectively.

The performance of the planar ring cavity was very similar to that of the linear cavity; see Fig. 5. This could be expected since the differences were related to the weak dependence of the mirror characteristics on the angle of incidence and the additional mirror used. While the slope efficiency obtained with the RISTRA cavity in Fig. 5 is almost the same, the threshold was significantly higher compared not only to the linear but also to the planar ring cavity. This can be attributed to the impossibility to use the RISTRA monolithic cavity off-axis in order to utilize the best position in the HGS crystal, to some damage of the AR coating of the SiO_2 wave plate established afterward, and to the lower OC signal reflectivity for p polarization.

C. Different Cavities with Large Pump Beam Diameter

Figure 6 shows the obtained input–output OPO characteristics with the three cavities at large pump diameter ($D_P = 5.35$ mm).

In this case HGS #3 was used and the linear cavity length was 51.2 mm. The mirror damage threshold was lower at larger beam sizes, and we had to trade off some of the mirror properties choosing fused-silica substrate for the ICs/BMs and CaF_2 for the OCs. These new mirrors showed better damage resistivity. The limit in terms of pump fluence was determined then by the damage threshold of the HGS #3 sample, which was chosen for its better overall homogeneity across its aperture. For HGS, we also observed that the damage resistivity in terms of fluence or intensity depends on the beam size [13].
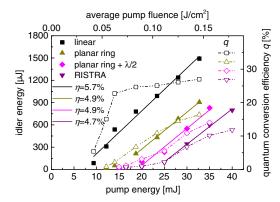
In this series of experiments a new uncoated MgF_2 zero-order half-wave plate, for which the Fresnel reflection was roughly 3% per surface, was used. To highlight its effect on the OPO characteristics we inserted the same wave plate in the planar ring cavity, with proper orientation so that no polarization rotation occurred: this is an additional case included in Fig. 6.

The linear cavity OPO threshold was substantially lower compared to the other cavities. This was due to the partial reflectivity (<41%) of the new OC at the pump wavelength, which means some additional amplification of the signal in the backward direction. This effect is impossible in the planar ring and RISTRA cavities since the pump is transmitted through the BMs. For this reason, rigorous comparison in the case of large pump beam size was only possible between the planar ring and RISTRA cavities. Nevertheless, reaching an output idler energy of 1.5 mJ at 6300 nm with the linear cavity (Fig. 6) was an important achievement since, as will be seen later, this was combined with much better focusability than previously demonstrated [10].

As could be expected from theoretical models [9], which give an expression for the OPO threshold, the pump retro-reflection has a stronger effect than modified feedback at the signal wavelength (as a result of the different mirror reflectivity at the signal wavelength in the three cavities). A direct confirmation for the effect of the pump retro-reflection is seen comparing Figs. 5 and 6. The mirrors used in the linear cavity for the small pump beam size (Fig. 5) had higher reflectivity at the signal wavelength, but the threshold, in terms of pump fluence, was higher than in Fig. 6. The somewhat lower slope efficiency for all cavities at large pump beam size in Fig. 6 can be attributed to the worse idler extraction, determined by the OC transmission at 6300 nm. However, it can be seen from Fig. 6 that the initial slope in the case of the linear cavity is much higher and saturation of the quantum efficiency is reached much earlier than in Fig. 5, again due to the second partial pump pass. The efficiency of this second pass in our specific case

where it was not intentional depends on the parallelism of the OC mirror (5' wedge according to specifications) because the pump reflection occurs to a great extent from the rear surface AR coating for the idler.

RISTRA presents the worst energy performance, but the idler slope efficiency is very close to that of the planar ring. The reasons for the increased threshold are related to additional losses: the new OC mirrors had stronger polarization dependence and the output coupling for the signal was higher in the RISTRA cavity due to the p polarization. Similarly, the BMs contributed to higher signal loss in the RISTRA cavity, there was an additional BM, and the half-wave plate introduced an additional signal loss of 6% per passage. The effect of the uncoated wave plate can be seen in Fig. 6 for the case in which it was included in the planar ring: the threshold was somewhere between the standard planar ring and RISTRA cavities; the slope remained, however, unchanged.

4. Output Beam Quality

The idler beam profiles were recorded by a SpiriconTMPyrocam III camera equipped with a LiTaO$_3$ pyroelectric detector (active area, 12.4 mm× 12.4 mm; element size, 0.1 mm × 0.1 mm). The software automatically evaluates the beam diameters at the $1/e^2$ intensity level. Several methods for calculation are included in the software menu, among them the ISO standardized second-moment σ beam width ($D_{4\sigma} = 4\sigma$), which was selected. The frame orientation option was enabled in some cases in which it was important to calculate the beam area (e.g., for evaluation of the pump intensity). For instance, in the pump profile measurements performed with the same instrument and shown in Fig. 1, the orthogonal eigenframe was rotated by 7° and 19° with respect to the horizontal/vertical directions (laboratory frame) in the case of small and large pump diameters, respectively.

In the actual idler beam measurements the frame orientation option was disabled because we were interested in having the results in the horizontal (H) and vertical (V) planes, which correspond to the critical (c) and noncritical (nc) plane designations for HGS. In addition, the intensity distributions displayed along the H (bottom) and V (left) axes were fitted with Gaussian functions, and the software provided two equivalent Gaussian beam diameters D_g. Beam diameters computed in this way were less sensitive to the aperture size selected for the fit compared to the $D_{4\sigma}$ method. The results should be close for beams with good quality, i.e., with low M^2.

The idler beam quality was studied with a 10 cm CaF$_2$ focusing lens. Its position depended on output beam size: normally the idler beam diameter was ≤10 mm on the lens, which is less than half the 1 in. lens diameter. The fitted Gaussian or second-moment beam waist data can be processed using different algorithms. Diameters (or radii) can be squared and fitted to a second-order polynomial function of the propagation coordinate z. M^2 is then calculated from the three coefficients obtained. With more sophisticated software, fitting of square root expressions can be applied without first squaring the data. This fitting procedure directly gives M^2 in the two planes. It results in smaller χ^2 values for the goodness of the fit. In the present case such fitting was always possible while the parabolic fit could lead to imaginary values for M^2. We used both procedures but concluded that the square root fitting is more reliable and stable against noise. The illustrating examples below were obtained using this procedure, while Table 1 compares the results obtained with both methods.

Due to the different cavity losses discussed in the previous section, the OPO threshold was different for the three types of cavities studied, but the slope efficiencies η were very close. Thus, we compared the idler characteristics at two to three times threshold for the two different pump diameters.

A. Different Cavities with Small Pump Beam Diameter

The M^2 measurement with the $L = 54.5$ mm linear cavity was carried out at pump energy of 9 mJ and idler energy ∼400 µJ, which according to Fig. 5 means three times the threshold. The results included in Table 1 indicate that focused intensities would be roughly 10 times lower than in the ideal case of a diffraction-limited Gaussian beam. Nevertheless, the focal spots would be ∼80 times smaller in area compared to [10], where the highest energy level (3 mJ for the idler) with such an OPO was achieved with large beam sizes and double pump/idler pass. Thus, although the output energy is ∼7.5 times lower in the present case, the potential focal intensities will be >10 times higher.

Quite unexpectedly, the signal beam profile, which was also measured in this specific case under identical conditions, showed worse quality (larger M^2 parameter). Using the square root fitting procedure for the Gaussian diameters we obtained M^2 = 6.1 and 10.7 in the horizontal and vertical planes,

Table 1. M^2 **Fitting Results for the Different Cavities in Two to Three Times Above Threshold Operation[a]**

Cavity	$D_P = 2.25$ mm, HGS #2				$D_P = 5.35$ mm, HGS #3			
	D_g		$D_{4\sigma}$		D_g		$D_{4\sigma}$	
	H	V	H	V	H	V	H	V
Square root expression and Levenberg algorithm								
Linear short	6.5	7.3	7.9	9	—	—	—	—
Linear	3	3.6	2.1	2.8	8.3	9.6	12.8	13.3
Planar ring	3.5	2.4	6.1	4.1	9.7	6.7	11	6.4
RISTRA	3.1	3.5	6.3	8.3	4.8	5.4	5	5.2
Quadratic expression and least-square algorithm								
Linear short	6.2	6.5	8.6	9.9	—	—	—	—
Linear	4.4	4.3	F	F	8	9.5	13	14
Planar ring	3.6	2.5	5.5	3.9	10.3	6.9	11.1	6.4
RISTRA	3.2	3.6	6.7	9	4.3	5.2	5.6	5.7

[a]F, fit procedure failed.

respectively. From the second moments the corresponding values were $M^2 = 7.5$ and 12. Thus, comparing with Table 1, it seems that M^2 is smaller in the critical plane only for the resonated signal.

It should be outlined here that in this case noise suppression in the data record for the idler was not optimum because the second procedure based on a parabolic fit failed (Table 1). Moreover, this represents the only case in the table in which second-moment fitting gave smaller values for the diameter compared to Gaussian fitting. In all other cases in Table 1 Gaussian fitting returned lower values for M^2, which can be compared with measurements in the literature by means of the knife-edge method. On the other hand, fitting of a quadratic instead of a square root expression resulted in very close M^2 values, except in this case when it failed; see Table 1.

The dependence of the idler beam quality on the pump/output energy was studied performing measurements at pump energies of 6 and 9 mJ, which corresponded to idler energies of 250 and 400 μJ, respectively. In this case denoted as "linear short" in Table 1, $L = 23$ mm; see Fig. 4. The results at pump energy of 9 mJ are included in Table 1. At pump energy of 6 mJ, using the square root method and the Gaussian diameters we obtained $M^2 = 5.4$ and 4.6 in the horizontal and vertical planes, respectively, or $M^2 = 6.3$ and 7 in the same planes with the second moments. Thus the deterioration of the idler beam quality does not show strong dependence on the pump level. As could be expected, the signal beam quality with the short linear cavity got also worse. It was measured only at a pump level of 9 mJ: using the square root method and the Gaussian diameters we obtained for the signal $M^2 = 13.4$ and 18.6 in the horizontal and vertical planes, respectively, and with the second moments we obtained $M^2 = 26.1$ and 20.6 in the same planes. The M^2 factor for the signal was two to three times larger than for the idler, similar to the standard $L = 54.5$ mm linear cavity.

The idler beam profile for the planar ring cavity was measured at pump energy of 9 mJ corresponding to idler energy of 360 μJ, i.e., close to three times threshold according to Fig. 5. The near-field (at 14 cm from OC) idler beam profile had Gaussian diameters of $D_{gH} \approx 2.91$ mm and $D_{gV} \approx 1.70$ mm in the two planes, while the corresponding second moments gave $D_{4\sigma H} \approx 4.61$ mm and $D_{4\sigma V} \approx 2.57$ mm (the values are approximate because they are in a frame rotated at ~4.7° from the laboratory frame; Fig. 7—top, left). The far-field (at 42 cm from OC) idler profile had $D_{gH} \approx 7.86$ mm and $D_{gV} \approx 5.42$ mm, while the corresponding second moments gave $D_{4\sigma H} \approx 10.47$ mm and $D_{4\sigma V} \approx 8.72$ mm (eigenframe at ~1.7° from laboratory frame; Fig. 7—top, right). Notwithstanding the observed ellipticity (larger diameter in the horizontal direction) the beam quality was not worse than with the linear cavity of the same length (Table 1). It was not possible to achieve a circular idler beam profile when the planar ring OPO was aligned for maximum output.
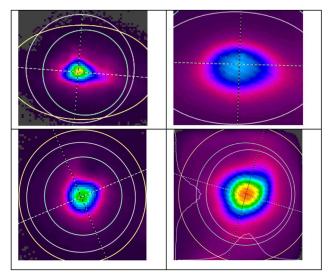

Fig. 7. Idler beam profiles with the planar ring (top) and RISTRA (bottom) cavities recorded at 14 cm (left) and 42 cm (right) from OC at small ($D_P = 2.25$ mm) pump diameter. The pump energy is 9 mJ for the planar ring and 12 mJ for the RISTRA cavity.

The idler beam profile from the RISTRA cavity was measured at pump energy of 12 mJ corresponding to idler energy of 330 μJ; see Fig. 5. Thus the idler output level was very similar to the 360 μJ idler energy for which the planar ring was characterized with this pump diameter.

The near-field (at 14 cm from OC) idler beam profile had Gaussian diameters of $D_{gH} \approx 2.29$ mm and $D_{gV} \approx 2.30$ mm in the two planes, while the corresponding second moments gave $D_{4\sigma H} \approx 3.33$ mm and $D_{4\sigma V} \approx 3.59$ mm (the values are approximate because they are in a frame rotated at ~22.7° from the laboratory frame; Fig. 7—bottom, left). The far-field (at 42 cm from OC) idler profile had $D_{gH} \approx 6.27$ mm and $D_{gV} \approx 5.83$ mm, while the corresponding second moments gave $D_{4\sigma H} \approx 8.64$ mm and $D_{4\sigma V} \approx 9.49$ mm (eigenframe rotated at ~16.2° from laboratory frame; Fig. 7—bottom, right). One can see clearly the effect of image rotation: the distribution is rather symmetric and the square-like shape highlights the 90° image rotation.

The corresponding M^2 measurements are shown in Fig. 8 and summarized in Table 1. There was no significant improvement with respect to the planar ring cavity for the small pump diameter. The only advantage of the RISTRA cavity seems to be the more symmetrical idler beam profile with closer M^2 values in the horizontal and vertical planes.

Figure 9 illustrates the idler temporal shape measured with a (HgCdZn)Te detector of 2 ns rise time. This raw measurement was not deconvolved with the detector response, but it shows nevertheless that the generated idler pulses were shorter than the pump pulses, which were measured by a 70 ps response time an InGaAs photodiode.

B. Different Cavities with Large Pump Beam Diameter

While the energy dependence with HGS #3 in the $L = 54.5$ mm linear cavity shown in Fig. 6 was
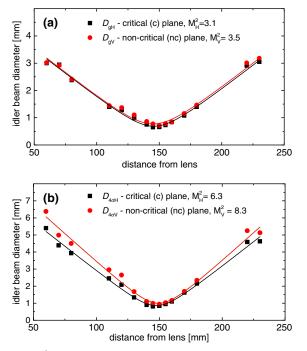
Fig. 8. M^2 fits (lines) to the experimental idler beam widths in terms of (a) Gaussian and (b) second-moment diameters in the two planes obtained with the RISTRA cavity at small ($D_P = 2.25$ mm) pump diameter and 12 mJ pump energy.

recorded at the best position in the sample, to avoid damage risk beam characterization was performed at a different position. The extrapolated OPO threshold for this position was ~12 mJ, but idler profiles were recorded at pump energy of 35 mJ, which is roughly three times threshold, while the idler energy was ~1 mJ, just as in Fig. 6.

The results of the M^2 fitting using Gaussian diameters and second moments are included in Table 1. As expected beam quality was worse compared to the small beam diameter, in agreement with theoretical models and previous experiments.

However, one should compare with other data with caution since, as already mentioned, in this configuration the HGS crystal was partially pumped in a
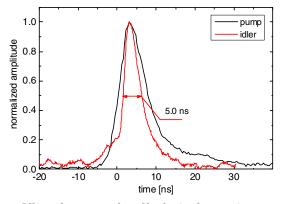

Fig. 9. Idler pulse temporal profile obtained at maximum energy with the RISTRA cavity using HGS #2 with a pump diameter of $D_P = 2.25$ mm.

second pass. Nevertheless, since only the signal is amplified in this second pass and the measured idler is generated only forward, keeping the condition to compare different cavities at the same time above threshold OPO operation is still meaningful as long as only the idler output is analyzed.

M^2 is <10 according to Table 1, or roughly three times better compared to [10]. The maximum idler energy reached in this configuration was 1.5 mJ (Fig. 6) compared to 3 mJ in [10]. Thus the focused fluence under same conditions will be 5.5 times higher in the present case. Cavity length was similar in [10], and while the 10.76-mm-long HGS crystal was pumped in double pass [10], the main reason for the improvement in terms of M^2 is related to the reduced D_P in the present experiment.

The idler beam profile using the planar ring cavity was also studied in a crystal position different from the best one used for the results in Fig. 6. The threshold (without using the wave plate) amounted to 15–16 mJ in this new position, and the measurements were performed at pump energy of 35 mJ corresponding to idler energy of 600 μJ. As with the small pump beam diameter, the output idler beam profile exhibited pronounced ellipticity, with much larger divergence in the horizontal plane. The near-field (at 19 cm from OC) idler beam profile had Gaussian diameters of $D_{gH} \approx 1.97$ mm and $D_{gV} \approx 1.96$ mm in the two planes, while the corresponding second moments gave $D_{4\sigma H} \approx 4.51$ mm and $D_{4\sigma V} \approx 3.00$ mm (the values are approximate because they are in a frame rotated at ~2.2° from the laboratory frame; Fig. 10—top, left). The far-field (at 56 cm from OC) idler profile had $D_{gH} \approx 10.3$ mm and $D_{gV} \approx 5.60$ mm, while the corresponding second moments gave $D_{4\sigma H} \approx 10.52$ mm and $D_{4\sigma V} \approx 8.42$ mm (eigenframe at ~1.7° from the laboratory frame; Fig. 10—top, right).

The results summarizing the evaluation of the M^2 parameter are included in Table 1. It can be concluded that the planar ring cavity without image rotation produces in both cases (small and large pump beam diameters) an elliptical idler beam with larger divergence in the walk-off (critical) plane in contrast to the linear cavity but also in contrast with the theoretical background behind the RISTRA concept.

The idler beam profile measurements with a larger pump beam diameter for the RISTRA reveal the effect of image rotation as can be seen in Fig. 10 (bottom), where wings extend clearly in two orthogonal directions: horizontal and vertical. Comparing the two records it can also be seen that divergence is similar in both directions. For this measurement the pump energy was about 42 mJ and the idler energy amounted to ~830 μJ.

The near-field (at 19 cm from OC) idler beam profile had Gaussian diameters of $D_{gH} = 1.90$ mm and $D_{gV} = 2.03$ mm in the two planes, while the corresponding second moments gave $D_{4\sigma H} = 3.46$ mm and $D_{4\sigma V} = 3.53$ mm (values in the laboratory frame, orientation disabled; Fig. 10—bottom, left). The far-feld (at 63 cm from OC) idler profile had
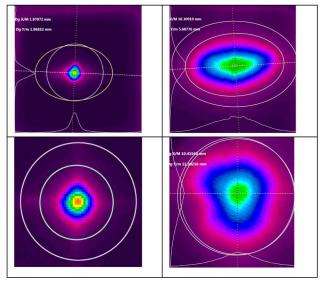
Fig. 10. Idler beam profiles with the planar ring (top) and RISTRA (bottom) cavities recorded at 19 cm (left) and 56/63 cm (right) from OC at large ($D_P = 5.35$ mm) pump diameter. The pump energy is 35 mJ for the planar ring and 42 mJ for the RISTRA cavity.

Fig. 11. M^2 fits (lines) to the experimental idler beam widths in terms of (a) Gaussian and (b) second-moment diameters in the two planes obtained with the RISTRA cavity at large ($D_P = 5.35$ mm) pump diameter and 42 mJ pump energy.

$D_{gH} = 10.41$ mm and $D_{gV} = 11.30$ mm, while the corresponding second moments gave $D_{4\sigma H} = 10.69$ mm and $D_{4\sigma V} = 10.97$ mm (values again in the laboratory frame; Fig. 10—bottom, right). Thus the idler divergence was lower compared to the planar ring cavity.

The corresponding M^2 measurements are shown in Fig. 11 and summarized in Table 1. It is obvious that in the case of large pump beam size, besides the more symmetric distribution, the idler beam quality with the RISTRA cavity has improved relative to the planar ring cavity.

5. Comparison with Previous Work and Conclusion

As already mentioned, in the present OPO eoe phase matching is dictated by maximum d_{eff} (lowest threshold) and phase-matching considerations. The signal is indeed walk-off decoupled from the low-quality pump, which is not single frequency. Thus, also keeping in mind the relatively short pump pulse duration, which is good for achieving a lower OPO threshold and avoiding crystal damage but counterproductive for the output beam quality, for the non-resonated idler one faces the worst RISTRA scenario. Hence, the M^2 values obtained (Table 1) can still be considered as promising. It should also be outlined that this is the first implementation of this concept, to the best of our knowledge, to a mid-IR OPO with nonoxide crystal pumped at 1064 nm. In this case, the resonated signal wavelength near 1280 nm results in more than two times larger Fresnel number compared to the 2 μm pumped OPOs with ZGP (Table 2). Also the number of round-trips is much lower in this work (Table 2); i.e., the cavity modes are less established (note that the lower quantum efficiencies are related to some extent to the imperfect
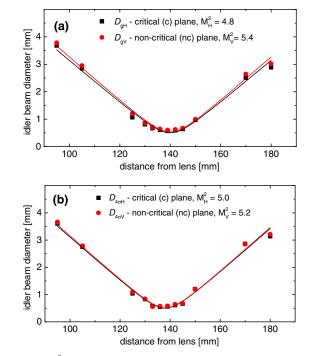
outcoupling of the idler, and the fact that the crystals were not AR-coated and that they showed absorption at 6300 nm).

One of the open questions in our experimental conditions is, if the RISTRA cavity improves the output beam quality due to the image rotation, which physical effect determines this enhancement. In this work, apart from the different cavities, we investigated the dependence of the idler beam quality on the pump beam diameter.

The pump beam size determines the range of angles (directions relative to the cavity axis) along which the signal oscillates in the plane-parallel cavity. Increasing the pump beam size supports higher-order spatial modes, which exhibit increasingly higher divergence than the fundamental mode, and the generated beam becomes highly multimode. As a result, increasing the pump beam diameter increased both the near-field signal and idler diameter and the far-field signal and idler divergence, leading to degradation of the output beam quality. Lower M^2 values (of the order of 3) were obtained for pump beam diameter of 2.25 mm with maximum idler energies reaching ∼0.4 mJ. For such a pump beam diameter, although the RISTRA cavity makes the idler profile slightly more symmetrical compared to the planar ring cavity and averages the M^2, in total it does not improve the beam quality. As a matter of fact, if we take the geometrical mean of the values in the two planes, we obtain from Table 1 a smaller value for the planar ring cavity ($M^2 = 2.9$) compared to the RISTRA cavity ($M^2 = 3.3$).

Table 2. Mid-IR OPOs Based on RISTRA Cavities Pumped by Multi-Frequency and Single- or Multi-Transversal Mode Structure Pump Sources for which the Beam Quality of the Output (M2) has Been Reported[a]

Reference	Pump	Crystal	Cavity	N	W	Signal	Idler
[5,6]	2050 nm, $M^2 \sim 1$, 20 ns, 72 mJ, 100 Hz, $D_P = 4.5$ mm	ZGP, type-I, eeo, θ = NA, l = 10 mm, $\rho_{S,I}$ = 11.4 mrad, AR(P, S, I)	L = 109 mm, $L*\sim$131 mm, $R_S = 50\%$, T_I = HT, $\lambda/2$:Al$_2$O$_3$, N_F:55	46	2.7%	3400 nm, 11.5 mJ, η:22%, q:26.5%, @ 3.6 × threshold: M_c^2: < 1.8, M_{nc}^2: < 1.8	5163 nm, not studied
[7,8]	2053 nm, $M^2 \sim 1$, 38 ns, 44 mJ, 100 Hz, $D_P = 3.75$ mm	ZGP, type-I, eeo, θ = 56°, l = 16 mm, $\rho_{S,I}$ = 11.8 mrad, AR(P, S, I)	L = 130 mm, $L*\sim$165 mm, $R_S = 65\%$, $T_I > 98\%$, $\lambda/2$:MgF$_2$, uncoated, N_F:36	69	5%	3012 nm, 10.25 mJ, η:29.7%, q:34.2%, @ 4.5 × threshold: M_c^2:1.38, M_{nc}^2:1.43	6450 nm, 5.67 mJ, η:16.3%, q:40.5%, @ 4.5 × threshold: M_c^2:1.74, M_{nc}^2:1.81
This work	1064 nm, $M^2 \sim 2$, 8 ns, 12 mJ, 10 Hz, $D_P = 2.25$ mm	HGS, type-II, eoe, θ = 50.26°, l = 13.44 mm, $\rho_{P,I}$ = 17.8, 16.8 mrad, AR(P, S)	L = 128 mm, $L*$ = 148.4 mm, $R_S = 72\%$, $R_I = 95\%$, $\lambda/2$:1.2 mm, SiO$_2$, AR, N_F:31	16	10.3%	1280 nm, not studied	6300 nm, 0.36 mJ, η:5.6%, q:17.5%, @ 2 × threshold: M_c^2:3.1, M_{nc}^2:3.5
This work	1064 nm, $M^2 \sim 2$, 8 ns, 42 mJ, 10 Hz, $D_P = 5.35$ mm	HGS, type-II, eoe, θ = 50.25°, l = 17.88 mm, $\rho_{P,I}$ = 17.8, 16.8 mrad, AR(P, S)	L = 128 mm, $L*$ = 154.8 mm, $R_S = 66\%$, $R_I = 83\%$, $\lambda/2$:1.6 mm, MgF$_2$, uncoated, N_F:175	15.5	5.8%	1280 nm, not studied	6300 nm, 0.8 mJ, η:4.7%, q:11.8%, @ 2 × threshold: M_c^2:4.8, M_{nc}^2:5.4

[a]N, number of round-trips; W, walk-off relative to pump diameter D_P, i.e., $W = 1 \times \tan \rho/D_P$; η, slope efficiency; q, quantum efficiency; HT, high transmission; reflectivity R and transmission T refer to OC; N_F is calculated assuming $2w_S = D_P$; NA, information not available.

Increasing the pump beam diameter to 5.35 mm leads to larger M^2, and this increase is more pronounced for the linear and planar ring cavities. According to Table 1, the increase of the pump beam diameter increased the geometrical mean M^2 for the planar cavity ~2.8 times to 8.1, while the corresponding increase for the RISTRA cavity was only 1.55 times to $M^2 = 5.1$ for $D_P = 5.35$ mm. At this M^2, the RISTRA cavity produced an idler energy of ~0.8 mJ.

The underlying physical effect behind the RISTRA concept is spatial walk-off. The magnitude of this effect (relative to the pump diameter) was varied in the two series of experiments performed, as can be seen from Table 2. In general this magnitude is much smaller compared to the RISTRA experiments with KTP discussed in the introduction, but in fact it could be made larger than in the ZGP OPOs included for comparison in Table 2. From the two series of experiments we saw no experimental evidence for the significance of the walk-off effect for the idler beam quality: although in linear cavities in most cases M^2 was slightly lower in the critical plane, in the planar ring cavities the idler beam was more divergent in this plane and the ellipticity was more pronounced. The RISTRA image rotation made the picture more symmetric assuming the better M^2 value, but this was for the noncritical plane. We also have no explanation for the worse beam quality of the (resonated) signal wave although such observations were limited to the linear cavity since the primary interest in this work was the idler in the mid-IR.

For practical applications, for instance, in tissue ablation, it is interesting to compute the fluence that is achievable in the focus of a lens with the different cavities employing the HGS crystal (as already mentioned this is the most successful material for mid-IR OPOs pumped at 1064 nm). Let us take a lens with focal length of 100 mm and assume the collimated idler beam at 6300 nm is circular with a diameter (at e^{-2} level) of $D_{I0} = ½''$ at the lens, i.e., half the lens aperture. A working distance of $f = 100$ mm is indeed realistic for such kinds of applications. Then the diameter in the focal plane will be $D_I = 4M^2\lambda_I f/\pi D_{I0}$ and the focal spot area—$\pi D_I^2/4$. Table 3 summarizes the results obtained for this area and the achievable focal average fluence.

The first three rows show results from this work, while the last row corresponds to the highest energy achieved in [10] albeit at much higher M^2. Table 3 takes into account the achieved maximum idler energy in each case (experimental values reported), limited in all configurations by optical damage. It can be seen that much higher focal fluences are achievable with the OPO configurations studied in this work compared to [10]. In addition, it can be expected that optical damage effects could be in principle overcome to some extent by improving the spatial beam quality of the beams (especially the resonated one if the pump source is the same).

Table 3. Focal Spot Areas Achievable with Different HGS OPO Configurations and Corresponding Average Fluence in Focus

Cavity	D_P [mm]	Idler Energy [mJ]	M^2 H/V	Focal Spot [mm²]	Average Fluence [J/cm²]
Planar ring	2.25	0.38	3.5/2.4	0.0272	1.4
	5.35	0.83	9.7/6.7	0.208	0.4
RISTRA	2.25	0.36	3.1/3.5	0.0352	1
	5.35	0.8	4.8/4	0.0832	1
Linear, double pump / idler pass [10]	9	3	28/31.5	2.88	0.1

The focal fluence can also be very high at small pump diameters when the output energy is limited but the Fresnel number is lower and the RISTRA design is not necessarily advantageous. However, the RISTRA cavity has definite advantages over the other cavities at high idler energies (large pump diameters), when such are required, providing not only lower M^2 values but also symmetric beam shape and equal focal distance in the two planes. An additional benefit of the RISTRA design is that ring cavities having nonplanar geometry are insensitive to small tilts of their cavity mirrors, which gives better positional stability.

Note that the achievable focal fluences calculated in Table 3 for the planar ring cavity are somewhat exaggerated due to the assumption of circular beam shape in the focusing lens position, while the actual idler output beams are elliptic (see Figs. 7 and 10). This is more pronounced for the small pump diameter. If one assumes that the larger beam diameter corresponds to ½″ at the lens, the achievable focal fluence with the planar ring cavity with small pump diameter will not exceed the corresponding value in Table 3 for the RISTRA cavity.

In future work it will be essential to decrease the OPO threshold with the RISTRA setup that exhibited the highest cavity losses, especially in the configuration with a large pump beam diameter. This will permit damage-free operation up to about four times threshold, where higher output energy can be expected [7,8]. At present no saturation (backconversion) is seen in the output energy dependence of the RISTRA OPO, and the quantum conversion efficiency obtained was the lowest of all cavities studied. The straightforward improvements to this goal include maximum outcoupling of the idler, optimized total losses for the signal—including reflectivity of all mirrors and transmission of the wave plate—and AR coating of HGS at the idler wavelength. A less trivial improvement will be the reduction of the crystal residual absorption at the idler wavelength and growing crystals with improved homogeneity and damage resistivity. Although higher M^2 values could be expected for operation at higher pump levels, one also anticipates that the advantages of the RISTRA concept become more pronounced. It will also be very interesting to study the present setup with different pump sources including such with similar beam quality but longer pulse duration as well as pump sources operating in the fundamental transversal mode. Single-frequency OPO operation with a single-frequency pump will be more challenging, but in principle it can be realized with a single-frequency seed diode at the signal wavelength.

References

1. V. Petrov, "Frequency down-conversion of solid-state laser sources to the mid-infrared spectral range using non-oxide nonlinear crystals," Prog. Quantum Electron. (to be published).
2. A. V. Smith and M. S. Bowers, "Image-rotating cavity designs for improved beam quality in nanosecond optical parametric oscillators," J. Opt. Soc. Am. B **18**, 706–713 (2001).
3. A. V. Smith and D. J. Armstrong, "Nanosecond optical parametric oscillator with 90° image rotation: design and performance," J. Opt. Soc. Am. B **19**, 1801–1814 (2002).
4. D. J. Armstrong and A. V. Smith, "Demonstration of improved beam quality in an image-rotating optical parametric oscillator," Opt. Lett. **27**, 40–42 (2002).
5. A. Dergachev, D. Armstrong, A. Smith, T. Drake, and M. Dubois, "3.4-µm ZGP RISTRA nanosecond optical parametric oscillator pumped by a 2.05-µm Ho:YLF MOPA system," Opt. Express **15**, 14404–14413 (2007).
6. A. Dergachev, D. Armstrong, A. Smith, T. Drake, and M. Dubois, "High-power, high-energy ZGP OPA pumped by a 2.05-µm Ho:YLF MOPA system," Proc. SPIE **6875**, 687507 (2008).
7. G. Stoeppler, M. Schellhorn, and M. Eichhorn, "Enhanced beam quality for medical applications at 6.45 µm by using a RISTRA ZGP OPO," Laser Phys. **22**, 1095–1098 (2012).
8. G. Stoeppler, M. Schellhorn, and M. Eichhorn, "Ho³⁺:LLF MOPA pumped RISTRA ZGP OPO at 3-5 µm," Proc. SPIE **8604**, 86040I (2013).
9. S. J. Brosnan and R. L. Byer, "Optical parametric oscillator threshold and linewidth studies," IEEE J. Quantum Electron. **15**, 415–431 (1979).
10. A. Esteban-Martin, G. Marchev, V. Badikov, V. Panyutin, V. Petrov, G. Shevyrdyaeva, D. Badikov, M. Starikova, S. Sheina, A. Fintisova, and A. Tyazhev, "High-energy optical parametric oscillator for the 6 µm spectral range based on HgGa₂S₄ pumped at 1064 nm," Laser Photon. Rev. **7**, L89–L92 (2013).
11. V. Petrov, V. Badikov, and V. Panyutin, "Quaternary nonlinear optical crystals for the mid-infrared spectral range from 5 to 12 micron," in *NATO Science for Peace and Security Series - B: Physics and Biophysics, Mid-Infrared Coherent Sources and Applications*, M. Ebrahim-Zadeh and I. Sorokina, eds. (Springer, 2008), pp. 105–147.
12. M. Eichhorn, G. Stöppler, M. Schellhorn, K. T. Zawilski, and P. G. Schunemann, "Gaussian- versus flat-top-pumping of a mid-IR ZGP RISTRA OPO," Appl. Phys. B **108**, 109–115 (2012).
13. V. Petrov, G. Marchev, A. Tyazhev, M. Beutler, V. Panyutin, M. Starikova, A. Esteban-Martin, V. Badikov, G. Shevyrdyaeva, D. Badikov, M. Reza, S. Sheina, and A. Fintisova, "Optical damage studies of mercury thiogallate nonlinear crystals for use in 1-µm pumped optical parametric oscillators," Opt. Eng. **52**, 117102 (2013).